

Deterministic modeling of driving and dissipation for ocean surface gravity waves in two horizontal dimensions

Jorge F. Willemsen

Rosenstiel School of Marine and Atmospheric Science, University of Miami, Miami, Florida, USA

Received 13 June 2001; revised 13 December 2001; accepted 7 January 2002; published 31 August 2002.

[1] Previous work introducing deterministic modeling of driving and dissipation to nonlinear surface gravity wave dynamics is extended to two horizontal spatial dimensions. It is shown that the wave spectrum rapidly develops into a form with two important features. First the spectral peak location is determined by the wind speed and shifts toward lower wave numbers as a function of time. This is due in part to nonlinear interactions, but it is also due to the functional form of the wind-forcing term. In addition, the spectrum rapidly develops an asymptotic power law tail in the downwind direction. The spectral exponent governing the asymptotics is sensitively dependent on the precise form of the dissipation term, and it can be “tuned” by adjusting that term in a quantitatively established manner. The angular dependence of the wave spectrum is also obtained. The strength and the role of the nonlinear interactions in the development of the spectral shape are studied in detail. The question of whether the wave amplitude statistics approach a Gaussian form is investigated. We find that a low-order odd moment is nonvanishing. *INDEX TERMS*: 4215 Oceanography: General: Climate and interannual variability (3309); 4522 Oceanography: Physical: El Niño; 4842 Oceanography: Biological and Chemical: Modeling; 4845 Oceanography: Biological and Chemical: Nutrients and nutrient cycling; *KEYWORDS*: deterministic modeling, deep water gravity waves, driving, dissipation, spectral evolution, angular spectrum

1. Introduction

[2] Several numerical results on the deterministic nonlinear evolution of a wide range of initial conditions utilizing *Krastiskii's* [1994] form of the Zakharov equation [Zakharov, 1966, 1968] have been reported by this author [Willemsen, 1998, 2001a, 2001b]. The present work extends the previous by considering the physically relevant case of two horizontal dimensions. It thus has the capability of computing angular spectra. Later in this section we will describe further objectives of the present research.

[3] First, however, we review key elements of the earlier publications. Although any desired initial condition may be specified for the deterministic equations, the present work utilizes initial conditions in the form of asymmetric Gaussian-modulated harmonic wave groups. Such idealized waveforms are an excellent laboratory, both theoretically and experimentally, for investigating effects of nonlinearity on wave steepening, and thus on the approach to wave breaking [Magnusson *et al.*, 1999; Banner and Tian, 1998].

[4] Unlike the case of Willemsen [1998], numerical instabilities developed in work by Willemsen [2001a] when certain initial conditions of the aforementioned type were prescribed. This was found to be caused by an excessive steepening of the slope due to wave-wave interactions, in qualitative agreement with the results of Banner and Tian.

[5] It was this numerical divergence which motivated Willemsen [2001b]: The physical description of ocean

waves is not complete until one introduces driving by the wind and dissipation of waves through wave breaking. The expectation that a dissipative component would stabilize the computations was realized in that paper. To do this, of course, it was necessary to introduce models for these processes. New progress is frequently reported in understanding wind driving, although much remains to be worked out, so this term is not extremely problematic. It will be discussed in detail in section 2.2. The situation regarding dissipation is considerably bleaker because of the broad range of small-scale phenomena involved in the breaking of even a single wave. Nevertheless, for years theorists and modelers have considered it useful to combine scaling arguments and experimental observations to construct working models of a dissipative term that represents the effects of the ensemble of microprocesses. A class of examples based on dimensional analysis was studied by Willemsen [2001b]. The suggested approach, stemming from the spectral behavior for k large is developed in detail in section 2.3.

[6] We now turn to several issues involved regarding the state of wave modeling. Why bother with a deterministic formulation at this point in time? In spite of the existence of Zakharov's deterministic equations since the 1960s, the practice has been to use a computational formalism that is analogous in its formulation to the Boltzmann equation of nonequilibrium statistical mechanics (e.g., WAM; an excellent review is given by Komen *et al.* [1994]). While these “transport” models have been extremely useful in practice and have instructed the wave modeling community, they truncate the physics in vital ways. First, they discard phase information although this information governs waveshapes

and interaction patterns. Further, having assumed that the phases are random, one proceeds to the assumption that the wave amplitude statistics (as encompassed in the probability distribution function, or “pdf”) are Gaussian. Seas with broadband spectra, however, are not characterized by any single length or timescale save the location of the spectral peak, and the asymptotic behavior is independent of that location. It is now known that processes with no favored scale more often than not lead to pdfs with asymptotic power law tails [e.g., *Balkovsky et al.*, 2001; *Baumann et al.*, 2000]. So it is appropriate to examine to what extent a wind-driven sea evolves a Gaussian pdf when this was not built in at the outset.

[7] The above remarks beg the question, “If more complete physical formalisms exist, why haven’t they been dominant?” At least part of the answer comes from computational requirements. In 1996, *Su et al.* [1996] reported on the status of wave modeling efforts as of that date. They found that the discrete interaction approximation (DIA) to the full WAM method introduced to speed up calculations gave directional transfer rates that differed significantly from those given by the full WAM. *Lin and Huang* [1996a, 1996b] had found, on the other hand, that Zakharov’s Hamiltonian equations [Zakharov, 1974] produced directional transfer rates in close agreement with the WAM results, but that the solutions took about 100–200 times longer to run than the DIA.

[8] The challenge, therefore, was to develop a calculation method which was both accurate and fast. The key ingredient given by *Willemsen* [1998] was the observation that the Krasitskii formulation [Krasitskii, 1994] of Hamilton’s equations are of convolution form, hence amenable to solution using very rapid Fast Fourier Transform (FFT) techniques. For example, integration of the nonlinear terms in the equations of motion requires $N^2 \times N^2$ calculations for N grid points; one factor accounts for the number of integrated points and output points, while the second arises from being in two horizontal dimensions. FFT methods reduce this to $N^2 \log N^2$ calculations, which is considerably faster for any reasonable N . This method together with ever increasing computational capability opens the way for a return to full physics modeling.

[9] In this paper we will use the full-physics formalism in two horizontal dimensions supplemented by models for driving and dissipation that are formulated in the same spirit as in other work. We have found that a version of the model described in detail below reproduces key features of a real wind-wave spectrum. For example, any initial condition develops a spectral peak and saturates into a long power law tail. The spectrum grows in the vicinity of the peak, with the location of the peak shifting to the red as a function of time (section 3.2.). It is found that the spectral exponent in the direction of the wind depends sensitively on the dissipation term, and a novel scaling relation of this term with the nonlinear interactions is described (as discussed in section 2.3). Angular dependence in the driving term leads to a highly angularly dependent spectrum (section 3.4). We find that the wave amplitude statistics, as described by several measures, are close to Gaussian yet sufficiently different that a third-order moment (specifically $\langle a^*(k', t) a(k, t) a(k, t) \rangle$ with symbols defined later) is significantly different from zero (section 3.3). The role of the nonlinear

interactions is described throughout section 3. An important conclusion (sections 3.2 and 3.6) is that the wind source term is at least as important in driving the spectral peak to the red as are the nonlinear interactions. The physical reason for this is remarkably simple.

2. Deep Water Gravity Wave Dynamics

2.1. Preliminary Considerations

[10] The equations governing surface waves may be obtained as a set of Hamilton’s equations from the energy functional for the problem. The *Krasitskii* [1994] form of these equations is obtained by making a systematic perturbation expansion, with the relevant expansion variable being the wave slope $k\zeta(k)$. The linear theory corresponds to retention of powers of ζ and ψ no higher than quadratic. The first correction term in the Hamiltonian is third order, and the second correction term is quartic. Thus one speaks of “three-wave and four-wave interactions.”

[11] The three-wave interaction term has no resonances in the limit of deep water ($kh \gg 1$). Thus it may be eliminated entirely by means of a canonical transformation. Explicit formulae are given by *Krasitskii* [1994] among others; this reference is singled out merely for consistency. The transformation has the effect of modifying the form of the fourth-order interaction term in the Hamiltonian, which does contain resonant interactions in deep water. However, it is not necessary to perform this transformation. The computational labor of retaining the three-wave interaction is quite small. Therefore in what follows it shall be left intact. The combination of third- and fourth-order interactions retained here corresponds to what would be called a fourth-order interaction had the canonical transformation been performed.

[12] Coefficients to be displayed below apply in the limit of deep water and in the absence of capillary effects. Direct numerical simulations within the framework of Boussinesq equations have been performed by *Pushkarev and Zakharov* [1996, 2000] retaining capillarity and finite water depth, but these cases will not be discussed here.

[13] To this order, then, the Krasitskii equations in deep water explicitly read

$$\begin{aligned} \frac{\partial \zeta_k}{\partial t} = & |k| \psi_k \\ & - \frac{1}{2\pi} \int dk_1 [|k||k_1| - k \cdot k_1] \psi(k_1) \zeta(k - k_1) \\ & - \int \int dk_1 dk_2 K_\zeta(k, k_1, k_2) \psi(k - k_1 - k_2) \\ & \zeta(k_1) \zeta(k_2) \end{aligned} \quad (1a)$$

$$\begin{aligned} \frac{\partial \psi_k}{\partial t} = & -g \zeta_k + \frac{1}{4\pi} \int dk_1 [k_1 \cdot (k - k_1) + |k_1||k - k_1|] \\ & \psi(k_1) \psi(k - k_1) \\ & + \int \int dk_1 dk_2 K_\psi(k, k_1, k_2) \zeta(k - k_1 - k_2) \\ & \psi(k_1) \psi(k_2). \end{aligned} \quad (1b)$$

In the above, all (wave number) k variables are two dimensional, although, for convenience, vector notation (e.g., $k \equiv \mathbf{k}$) has been suppressed. Additionally, g is gravitational acceleration. Since the velocity potential and

the displacement are real quantities, their Fourier transforms must satisfy the conditions $\psi(k) = \psi^*(-k)$, $\zeta(k) = \zeta^*(-k)$, where the asterisk denotes complex conjugation.

[14] The integral kernels K_ζ and K_ψ above are explicitly

$$K_\zeta = \frac{1}{8p^2} |k| |k - k_1 - k_2| \{ |k| + |k - k_1 - k_2| - |k - k_1| - |k - k_2| \} \quad (2a)$$

$$K_\psi = \frac{1}{8p^2} |k_1| |k_2| \{ |k_1| + |k_2| - |k - k_1| - |k - k_2| \}. \quad (2b)$$

[15] Equations (1) and (2) govern the dynamics of the wave field in the absence of driving and dissipation. Their convolution form has been discussed extensively by *Willemssen* [1998, 2001a, 2001b]. These equations will now be supplemented with expressions for wave growth and dissipation. As discussed by *Willemssen* [2001b], the models utilized are based primarily on observation and/or modeling with first principles underpinnings where available.

2.2. Growth Terms

[16] Although the following discussion has been published by *Willemssen* [2001b], it will be repeated for the reader's convenience. There are four issues to deal with in formulating a phenomenological model for wave growth in response to a wind. First, there is the functional form of the driving itself. Next is the problem of parameterizing the wind velocity. Then, one must ensure that the wind drives waves appropriately depending on their phase speed. Finally, one must adequately parameterize the directional properties of the wind in two horizontal dimensions.

[17] The growth of a wave field produced by wind-forcing is often described in terms of the growth of the energy, e.g., $dE/dt = \alpha(U) E$, in which $\alpha(U)$ is a function of the wind speed U . Considering *Belcher and Hunt* [1993] for concreteness, however, the computed growth function may also be written as $\partial\zeta_k/\partial t \propto u_*^2 \zeta_k$, where u_* denotes the wind friction velocity. Considering further *Cohen and Belcher* [1999], the implicit proportionality 'constant' is not a constant at all, but depends upon factors of the form $(U(\lambda)/c_k - 1)$, where two separate length scales pertinent to their analysis are here abbreviated (λ), with $U(\lambda)$ computed according to a logarithmic velocity profile. Here c_k is the phase velocity of a wave with wave number k . The form of these factors stems from the fact that their calculation has been performed in a frame moving at the phase speed of the spectral component $\zeta(k)$ and one must transform back to the "laboratory" frame in which the dynamics is evaluated. This change of frame produces growth rate factors similar to those introduced by *Al-Zanaidi and Hui* [1984]. For the purposes of this paper, we will simply introduce a "parameter" U (in meters per second) in a driving function similar to that of *Al-Zanaidi and Hui* as refined by *Donelan and Pierson* [1987] and *Donelan* [1999] based upon experimental observations,

$$\frac{\partial\zeta_k}{\partial t} \propto (U \cos \varphi/c_k - 1) |U \cos \varphi/c_k - 1| \omega_k \zeta_k. \quad (3)$$

The formulas written by *Cohen and Belcher* contain additional factors which they denote by β and γ . These involve further U/c dependencies which give rise to nontrivial behavior as one varies these ratios. Although one

is studying a growth term, in a regime roughly corresponding to $U/c < 1$ ("roughly" because there are two separate length scales involved), wave suppression occurs.

[18] This damping phenomenon is generally considered physically plausible. More generally, the wind should cause waves with phase velocities smaller than its velocity to grow and cause waves with larger phase velocities to be diminished (which is the above *Cohen-Belcher* result), and waves with phase velocities opposite to the wave direction should also diminish. According to *Belcher and Hunt* [1993] the last requirement is automatically satisfied since the transformation $c \rightarrow (-c)$ produces the desired diminution once all of the dependencies have been exhibited.

[19] Going beyond the simple replacement $c \rightarrow (-c)$, we have introduced an angle φ between the wind direction and the wave direction in equation (3), and let the phase velocity always be a positive quantity; that is, c_k will refer to the wave speed rather than its velocity. It is readily verified that this functional form, which has minimal mathematical complication, satisfies all of the aforementioned constraints by virtue of the factor which is an absolute value. *Donelan* [1999] has also observed that the numerical coefficient α in equation (3) depends on the sign of the first bracketed quantity, in accord with the results of *Cohen and Belcher* [1999]. For the purposes of this investigation this refinement has not been adopted explicitly. Nonetheless, there is an "effective" change of strength which arises in the following manner. Consider the limiting case $\cos \varphi = -1$. The first bracketed term is negative. The "abs" term is positive, and its magnitude is $(U/c + 1)$, which is stronger than any case for which $(U \cos \varphi/c - 1)$ is positive.

[20] Thus, for the work to be described in this paper, the DP model has been selected to model the growth. There are several reasons for this choice. First, it displays the correct qualitative physics in the sense that it satisfies the criteria enumerated above. In addition, it is this author's belief that while the correct "driving" formulation for $\cos \varphi < 0$ is still lacking, some damping effect in this regime should be present in the model. Thus the DP form is certainly no worse than that of *Cohen and Belcher* [1999] in the opposing wind situation. Finally, for purposes of preliminary exploration, the DP model is useful because it is computationally much simpler than the model of *Cohen and Belcher*. No attempt is made in the work presented here to relate the nominal wave speed U to U_{10} or anything else; it is a parameter for the calculations, but it can be refined in future work.

[21] A comparison of the *Cohen-Belcher* model [*Cohen and Belcher*, 1999] and the DP model in the along-wind direction is shown in Figure 1. Qualitatively, the models are very similar provided the wind speed is larger than the phase speed. Numerically, the *Cohen-Belcher* model allows no "free" parameters (although the derivation is for neutral stability conditions) whereas the DP model allows at least one adjustable parameter. As can be seen in Figure 1, this parameter has been chosen to accelerate wave development relative to *Cohen and Belcher* in order to reduce computational time. We will discuss the significance of this accelerated development in section 2.4.

2.3. Dissipation Terms

[22] As was the case for driving, the motivation for the dissipation terms has been discussed at length by *Willemssen*

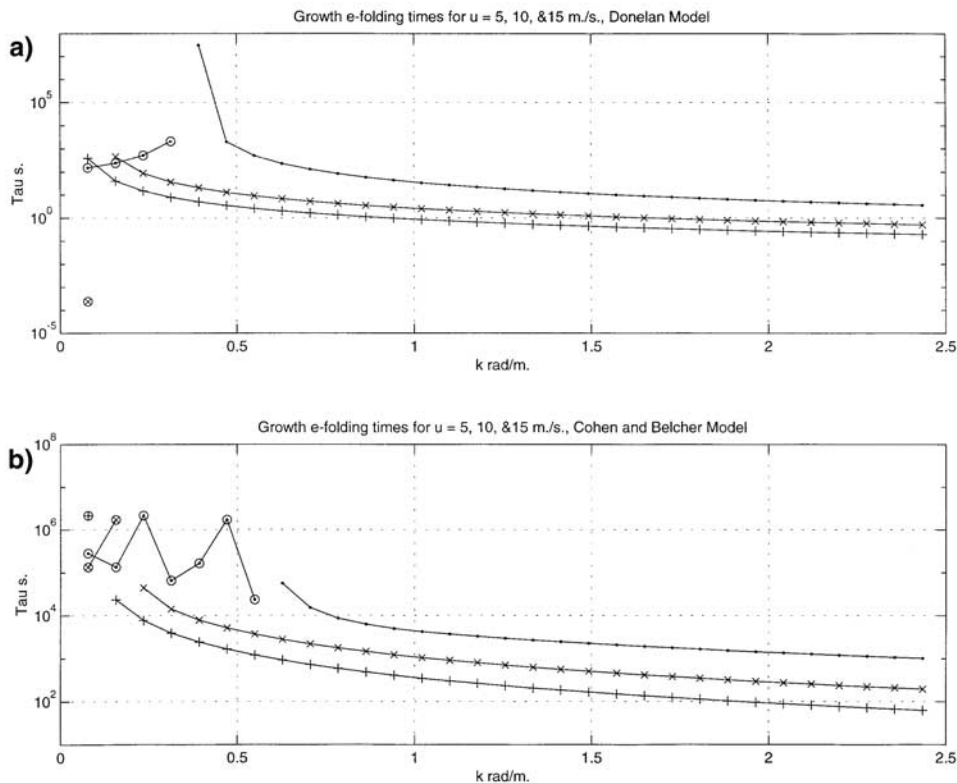


Figure 1. Growth e-folding times (time it takes to grow by a factor of e). (a) Donelan-Pierson Model; (b) Cohen-Belcher Model. Circles around points denote negative rates, i.e., damping rather than growth. The sign has been changed so they can appear on the logarithmic plot.

[2001b]. Here we present an abbreviated version of that discussion. Within the present formalism, ordinary viscous dissipation takes the functional form

$$\partial \psi_k / \partial t = -\nu k^2 \psi_k,$$

where ν denotes the kinematic viscosity. Our goal is to consider suitable additional terms which model wave breaking as a form of dissipation. We approach the construction of such terms in two steps.

[23] First, the combination $\omega_k \psi$ satisfies the dimensional constraints. Then, if we restrict the possible factors which describe the dissipation to include g (gravitational acceleration), wave number k , and ψ itself, we need to construct a dimensionless function of these three quantities. In $d = 1$ we have considered $f(k^5 |\psi|^2 / g)$, while in $d = 2$ we may consider $f(k^7 |\psi|^2 / g)$.

[24] Following the spirit of arguments advanced by *Kitaigorodskii* [1962], *Zakharov* [1968], and *Phillips* [1985], we invoke a power law dependency for the dissipation function

$$f(y) = y^\chi.$$

In work by *Willemssen* [2001b], numerical experiments revealed that the choice of χ influences the asymptotic spectral tail. We now develop these observations by performing a systematic set of numerical experiments in which χ is varied.

[25] Figure 2 encapsulates the results from such a series of numerical experiments in which the exponent χ used to parameterize the dissipation function in the form

$$\frac{\partial \psi_k}{\partial t} \propto -\beta \omega_k \psi_k \left(k^7 |\psi|^2 / g \right)^\chi \quad (4)$$

was varied. For each value of χ the dynamical model was run and the asymptotic spectral exponent ρ , as defined in

$$|\zeta|^2 \propto |k|^{-2\rho},$$

was calculated.

[26] Given the values of χ and ρ , the asymptotic scaling properties of the third- and fourth-order nonlinear terms, and that of the dissipation, are evaluated. For example, in one set of trials (fixed χ as input and ρ as output) we would conclude that

$$D \rightarrow (k^{7-2\rho-1})^\chi,$$

in which D refers to the RHS of equation (4). This expression takes into account both the superficial powers of k present in D and the “implicit” powers due to the presence of $|\psi|^2$. The same scaling is performed on the nonlinear terms, and the resulting exponents are plotted against one another. (Note that to an excellent degree of approximation, the calculations indicate that $|\psi|^2 \propto k^{-1} |\zeta|^2$.)

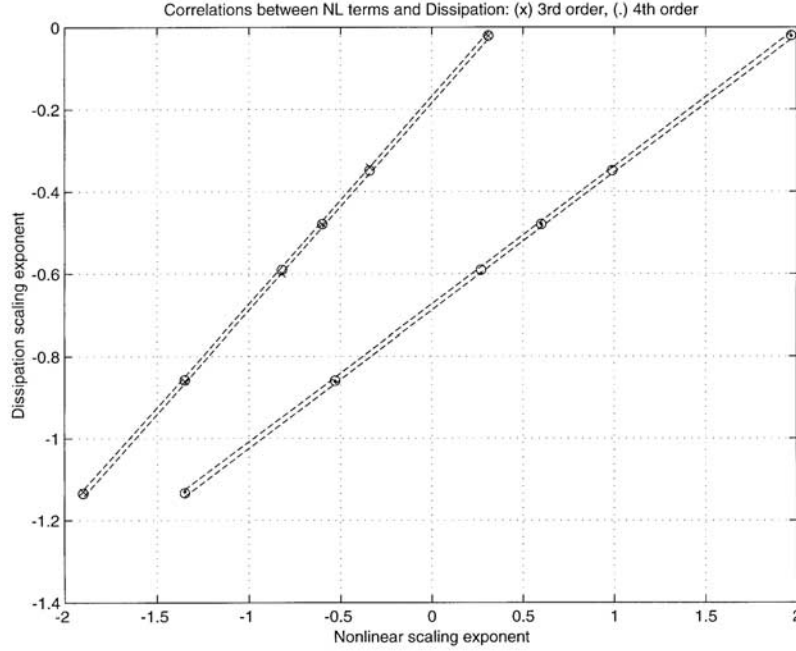


Figure 2. Scaling relation between the strength of the dissipation and the third and fourth order nonlinear interaction terms.

This observation may help in providing a physical interpretation for the argument of the function F : It behaves like $k^4 |k\zeta|^2$; that is, it is proportional to the square of the wave slope.)

[27] Figure 2 demonstrates that the above scaling properties correlate: The dissipation exponent tracks linearly with the nonlinear exponents. In each curve the circles correspond to least squares fits. (The dashed lines correspond to confidence levels defined as those within which at least 50% of the predictions lie under the assumption that the data are independently normally distributed with constant variance. They were computed using the Matlab “polyfit” routine.) At present we have no theory for this observation from our “computer experiment,” although we believe there must be one and it is being actively pursued.

[28] It is then a matter of interpolation to obtain the χ value which corresponds to whatever value of ρ one wishes. The results in this paper are a consequence of choosing $\rho = 2$, i.e., spectral exponent 4, which leads to a value for χ which we round to $2/3$. This choice was made in view of Banner’s observations [Banner, 1990], which are possibly reconciled with the famous $7/2$ law if one takes into account that this law was derived for the angle-averaged spectrum, whereas Banner’s exponent applies in the downwind direction. Results regarding angular dependencies will be addressed later.

[29] The key point here is that one may “tune” the dissipation in order to produce results which are in accordance with a set of observations, much as was done by Tolman and Chalikov [1996] within a third-generation WAM model, and more generally by Banner and Young [1994] as well. Further experimentation has revealed that the above correspondences are robust to changes in the parameters α and β , and additionally to the initial conditions

and the wind speed. This was also observed to be the case in $d = 1$ [Willemssen, 2001b].

2.4. How Do We Know That We Are Actually Driving and Dissipating the Ocean Surface?

[30] In what follows an abbreviated version of the dynamical equations is shown. The terms involving the Hamiltonian H are simply Hamilton’s equations. In addition the full dependencies of the driving and dissipation functions have been suppressed. Thus the model equations read

$$\frac{\partial \zeta_k}{\partial t} = \frac{dH}{d\psi_k^*} + \alpha \Gamma(k, U) \omega_k \zeta_k, \quad (5a)$$

$$\frac{\partial \psi_k}{\partial t} = -\frac{dH}{d\zeta_k^*} - \nu k^2 \psi_k - \beta \Delta(k, \psi) \omega_k \psi_k. \quad (5b)$$

The problem being addressed arises from questions like the following: “Can one prove that $\alpha \Gamma(k, U)$ causes the energy in the system to grow, while $\beta \Delta(k, \psi)$ causes the energy in the system to diminish?” The consistent way of verifying that non-Hamiltonian terms are in fact doing what they are supposed to be doing (driving and dissipating) has been recorded in Landau and Lifshitz’ “Mechanics” [Landau and Lifshitz, 1960]. While this may be obvious for exactly integrable systems, the issue warrants investigation when the system can only be solved numerically. Although the Landau-Lifshitz argument was supplied for a Lagrangian system, the method is readily adapted to describe a Hamiltonian system. The key to the method is to show that the driving and dissipation terms in the time derivative of the total energy functional are of definite sign. An example utilizing the linearized theory, the driving term, and viscous damping was presented by Willemssen [2001b]. The procedure has been carried out for the full model, but it is uninteresting except that one learns that the argument of the

function $f(y)$ describing dissipation must depend on $|\psi|$ and not on ψ , $\text{Re } \psi$, or $\text{Im } \psi$ separately, possibilities which were entertained in that paper.

2.5. Justification of Use of “Unphysically” Large Driving and Dissipation Coefficients Through Scaling Arguments

[31] First consider a central quantity in the detailed considerations which will follow, the spectral density $S(k) = |\zeta(k)|^2$. Based on the equation of motion satisfied by ζ it follows immediately that (at each k)

$$\frac{dS}{dt} = 2 \left\{ \alpha \Delta(k, U) \omega_k S + \text{Re} \left[\zeta \frac{\delta K}{\delta \psi} \right] \right\}.$$

This expression reflects the fact that the potential energy is independent of ψ . (It also reflects the fact that within the undriven linear theory, $\alpha = 0$, $S(k, t)$ oscillates with frequency $2\omega_k$ for a general solution of the form $\zeta = \zeta_+ e^{i\omega t} + \zeta_- e^{-i\omega t}$. The nonlinear interactions are contained in the second term on the RHS.

[32] Let the numerical coefficient α refer to that used in the numerical integration of the equations of motion, which give rise to $\zeta(k, t)$ and $\psi(k, t)$ dependencies. Introduce a more realistic coefficient which is much smaller than the one used for reasons explained earlier, say $\alpha = \lambda \alpha^0$ with $\lambda \gg 1$. Now, since the kinetic energy functional is homogeneous of degree 2 to all orders of perturbation theory, it follows that if $\psi = \lambda \psi^0$, while ζ remains unscaled, $\zeta = \zeta^0$, we obtain

$$\lambda^{-1} \frac{dS^0}{dt} = 2 \left\{ \alpha^0 \Delta(k, U) \omega_k S^0 + \text{Re} \left[\zeta^0 \frac{\delta K^0}{\delta \psi^0} \right] \right\}.$$

Physically, the meaning of the above equation is clear. The realistic growth coefficient leads to temporal evolution of the spectral density at a stretched time $\tau = \lambda t$, provided the Hamiltonian terms in $d\zeta/dt$ are scaled by λ . This latter step reflects the fact that through the equations of motion the velocity potential turns out to be correspondingly large when α is used in the calculations, so $\psi^0 = \lambda^{-1} \psi \ll \psi$. Note that the similar scaling of the two terms on the RHS indicates that the nonlinear interactions are in no way “underevaluated” through the use of α in the numerical calculations. Note also that in practice there is no need to recompute these terms dynamically. They are available as a result of the original calculation and can be scaled trivially.

[33] The situation regarding the rate of change of the energy is similar but not identical. In order to examine this rate, we take the “realistically scaled variables” as our starting point, and we examine the potential and kinetic energy contributions separately:

$$\begin{aligned} \frac{dU^0}{dt} &= \int dk \left[\alpha^0 \Gamma(k, U) \omega_k \zeta_k^0 \frac{\delta U^0}{\delta \zeta_k^0} + \frac{\delta U^0}{\delta \zeta_k^0} \frac{\delta K^0}{\delta \psi_k^{*0}} \right] \\ \frac{dK^0}{dt} &= \int dk \left[\alpha^0 T(k, U) \omega_k \zeta_k^0 \frac{\delta K^0}{\delta \zeta_k^0} - \beta^0 \Delta(k, \psi) \omega_k \psi_k^0 \frac{\delta K^0}{\delta \psi_k^0} \right. \\ &\quad \left. - \frac{\delta U^0}{\delta \zeta_k^0} \frac{\delta K^0}{\delta \psi_k^{*0}} \right]. \end{aligned}$$

Viscous dissipation has been neglected in these equations. It is numerically negligible compared to the “wave-breaking” $\beta \Delta$ dissipation terms.

[34] Applying the inverse of the scaling transformations described above, we obtain

$$\begin{aligned} \lambda^{-1} \frac{dU}{dt} &= \lambda \int dk \left[\alpha \Gamma(k, U) \omega_k \zeta_k \frac{\delta U}{\delta \zeta_k} + \frac{\delta U}{\delta \zeta_k} \frac{\delta K}{\delta \psi_k^*} \right], \\ \lambda^{-3} \frac{dK}{dt} &= \lambda^{-3} \int dk \left[\alpha T(k, U) \omega_k \zeta_k \frac{\delta K}{\delta \zeta_k} - \beta \Delta(k, \psi) \omega_k \psi_k \frac{\delta K}{\delta \psi_k} \right] \\ &\quad - \lambda \int dk \frac{\delta U}{\delta \zeta_k} \frac{\delta K}{\delta \psi_k^*}. \end{aligned}$$

Here we have introduced a further scaling $\beta = \lambda^{1-2\chi} \beta_0$ to account for the ψ dependence of the dissipation term, $\Delta(k, \psi) = \lambda^{2\chi} \Delta(k, \psi_0)$.

[35] Evidently the homogeneity arguments employed to study dS/dt do not apply in exactly the same manner. However, notice that the sum $d/dt (U^0 + K^0)$ does not contain the right-most member present in each term separately. They cancel. This cancellation suggests that we may implement the following procedure. In simulation variables, the “effective” potential energy equation will be taken to be

$$\frac{dU}{dt} = \int dk \left[\alpha \Gamma(k, U) \omega_k \zeta_k \frac{\delta U}{\delta \zeta_k} \right],$$

while the “effective” kinetic energy equation will be taken to be

$$\frac{dK}{dt} = \int dk \left[\alpha T(k, U) \omega_k \zeta_k \frac{\delta K}{\delta \zeta_k} - \beta \Delta(k, \psi) \omega_k \psi_k \frac{\delta K}{\delta \psi_k} \right].$$

We have eliminated the terms which cancelled in the original equation for dH^0/dt . The sum of these “effective” equations correctly yields

$$\frac{dH}{dt} = \int dk \left[\alpha T(k, U) \omega_k \zeta_k \frac{dH}{dz_k} - \beta \Delta(k, \psi) \omega_k \psi_k \frac{dH}{dy_k} \right].$$

If we work backwards, upon scaling the effective U and K evolution equations in order to describe the system in the “reasonable” variables, we will obtain exactly the same form of the equations in those variables. They are not true equations. Nevertheless, the sum is a true equation for dH^0/dt . In summary, we may conclude that $dH^0/d\tau = dH/dt$.

[36] These results succinctly demonstrate that scaling the numerical coefficients that enter into the driving and dissipation terms can be absorbed by a stretching of the time $t \rightarrow t\lambda$ together with a scaling of the velocity potential. Thus our choice of a Donelan-Pierson coefficient in the driving term which is considerably larger than values that emerge from the theory of *Cohen and Belcher* [1999] does not alter the basic physics of the problem. We can recover the Cohen and Belcher values by the scaling arguments above.

[37] As a final note, recall that the work in this paper was based upon a value $\chi = 2/3$. Thus the dissipation

coefficient $\beta_0 = \lambda^{1/3}\beta$, whereas the driving coefficient $\alpha_0 = \lambda^{-1}\alpha$, with $\lambda \gg 1$. However, while in the “reasonable” system, the dissipation coefficient is larger than it is in the simulated system, the overall dissipation function is smaller, $\beta_0\Delta(k,\psi_0) = \lambda^{-1}\beta\Delta(k\psi)$, as is physically plausible: less growth, smaller velocity potential, and less dissipation.

3. Results From a Model

3.1. Formulation of Calculations

[38] There is only one “trick” involved in passing from the $d = 1$ version of the FFT computational scheme to $d = 2$. One must assign a two-vector to each site of a two-dimensional grid. If we think of the grid as a matrix, because this is extremely useful for performing the calculations, we must have two quantities at each matrix element. One way to do this is to formulate the wave number vector as a complex variable $\mathbf{k} = (k_x, k_y) = k_x + ik_y$. All other manipulations are straightforwardly converted, e.g., using Matlab function `fft2` instead of `fft`, although of course the generalization is not confined to Matlab implementation.

[39] The fully nonlinear model of equations (5a) and (5b) has been run in $d = 2$, augmented by the DP driving formulation with an overall numerical coefficient α , and with several dissipation terms of the form described extensively above, multiplied by an overall coefficient β . While several values of these parameters have been explored, we report here only the specific choices $\alpha = 0.025$ and $\beta = 7.8e-3$. The time integrations were done using a variable time step Runge-Kutta (4,5) solver, specifically Matlab function “ode45”. Since the present investigations are in “research” rather than “production” mode, code optimization was not an issue here beyond successfully implementing the FFT technique. Future work can surely strive for even faster codes using any one of a number of techniques including different computational packages.

[40] The domain of the calculation consists of a two-dimensional grid with 64×64 points in wave number space. The wave numbers were discretized within this domain such that the slowest waves had phase speeds of 2 m s^{-1} . This determines the spacing dk , from which a spatial discretization parameter $dx = 1/(dk*64) = 1.25 \text{ m}$ follows.

[41] The initial condition for the work reported here is a cosine function modulated by a Gaussian envelope with different degrees of falloff in the x and y directions, $\cos(\kappa x) \cos(\kappa y) \exp(-\gamma_1 x^2) \exp(-\gamma_2 y^2)$, with numerical parameter values $\kappa = \pi/20$, $\gamma_1 = 0.0015$, and $\gamma_2 = 0.006$. As mentioned earlier, the main motivation for this is that initial conditions such as these led *Banner and Tian* [1998] to observe strong sensitivity to initial slope as a parameter governing likelihood of wave breaking. Other cases have been investigated but the results will not be discussed here. It has been found that past very early times there is little sensitivity to the precise parameterization of such functions given that the dissipation term now cuts off small wavelength instabilities which were interpreted as “breaking” events [Willemssen, 2001a].

[42] The calculation method inherently uses periodic boundary conditions, so the domain should be visualized as the surface of a torus. It may be useful to think of an

eastward moving wave as propagating along one great circle and a northward moving wave as propagating along the other. With the discretization spacing dk as indicated above, these great circles have a circumference of 80 m. Two observations regarding this spatial domain may be helpful in interpreting the results to follow. First, since under a steady wind the waves are forced initially in the wind direction, going “around and around” the torus mimics prolonged and persistent wind action. There is some “leakage” into and out of the cross-wind direction which can be thought of as “copies” of the region being studied responding in the same manner to the wind. Secondly, we should note that buoy measurements which are responding to a very local environment are used to infer directional spectra in field work.

3.2. Spectral Evolution

[43] Before viewing results from the model, it is useful to reexamine Figure 1a, which portrays the e-folding time (time it takes to evolve by a factor of the natural number $e = 2.7183$, also known as “the time constant”) associated with the DP driving function in the downwind direction as a function of wave number,

$$\tau(k) = [\alpha(U/c_k - 1) \text{abs}(U/c_k - 1)\omega_k]^{-1}.$$

The sharp peak seen in the curve for $U = 5 \text{ m s}^{-1}$ occurs at the discretized wave number which is closest to satisfying $U = c_k$. The time constant is singular at that precise point. Symbols with circles around them correspond to waves that are suppressed because they are traveling faster than the wind. (These are nevertheless depicted as positive so as to appear in the semilog plot.) Points which are not circled correspond to modes that can grow in this windfield.

[44] In the work reported here, $U = 10 \text{ m s}^{-1}$ was chosen for purposes of illustration. Notice that within 1 s, modes right down to 0.5 rad m^{-1} have experienced 1 e-folding growth for the value of α that was selected. The whole curve slides up and down as α is varied. Comparing Figure 1a with Figure 1b it is evident that there are orders of magnitude difference between the curves generated using the α of this paper and those which emerge without adjustment from the Cohen-Belcher theory. As was explained in detail in section 2.5, this discrepancy has no physical significance provided variable scalings are done at the end of the calculation.

[45] An important experimental observation during wave growth under fetch-limited conditions is downshifting of the spectral peak as a function of time. The theoretical explanation most often focuses on the effects of nonlinear interactions, which “mix” the spectral components [see, e.g., *Komen et al.*, 1994; *Hara and Mei*, 1991]. Figure 1 strongly suggests that this is not the full story. In brief, short waves grow rapidly and saturate. Longer waves take longer to grow. As they do so the spectral peak drifts toward lower wave numbers at an ever slower rate. In short, a significant part of the shift is due to the wave number dependence of the driving term.

[46] We are now ready to turn to Figure 3. This is a log log plot of the spectrum averaged over 5-s intervals at successive times. In ascending order, these are 1–5, 45–50, 95–100, 195–200, 295–300, 395–400, and 495–500 s.

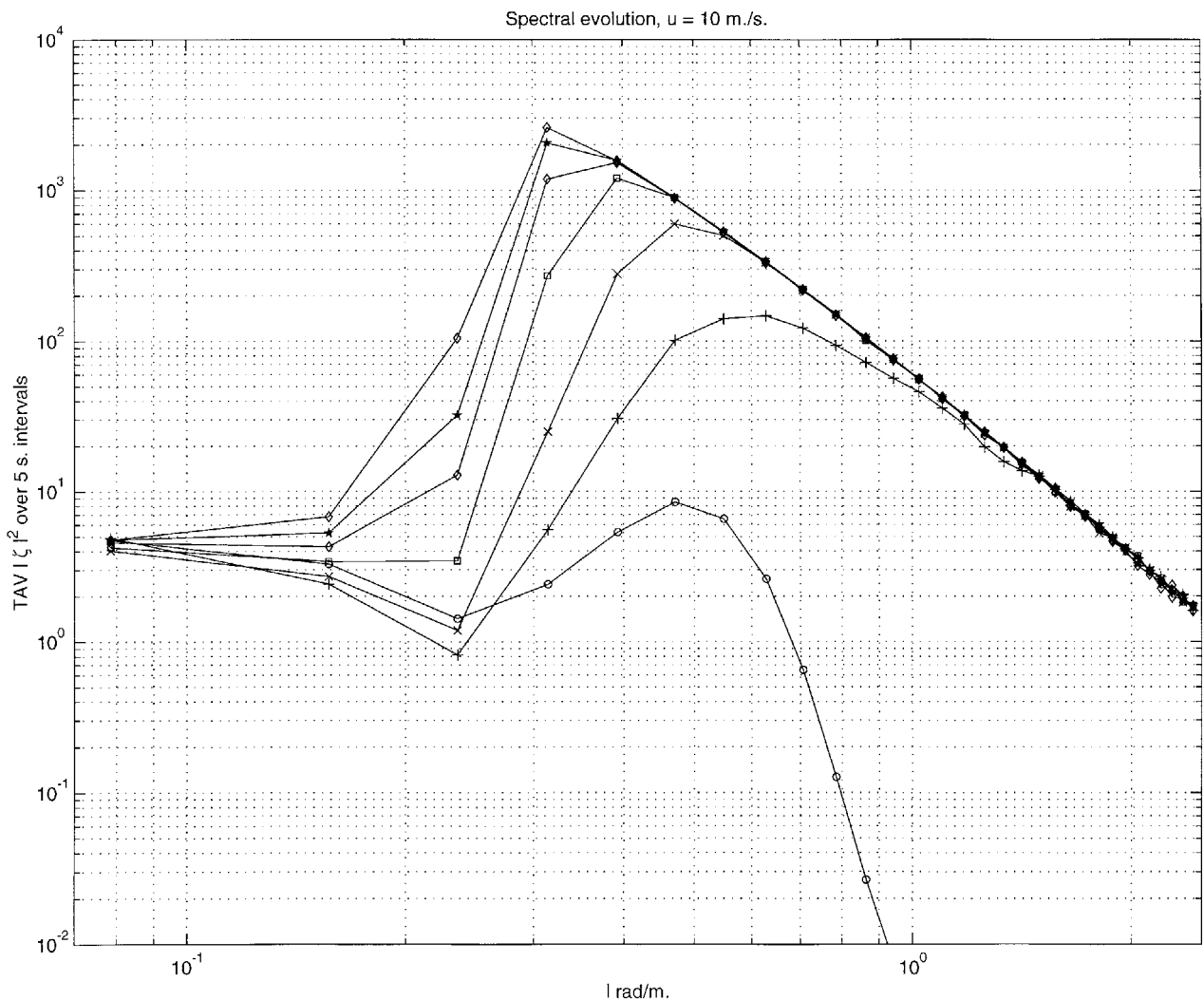


Figure 3. Spectral evolution based upon a choice of the dissipation exponent selected to produce k^{-4} asymptotics. The TAV refers to time averaging over the time intervals corresponding to the curves, which are marked as follows: (circles) 0–5 s, (plus signs) 45–50 s, (crosses) 95–100 s, (squares) 195–200 s, (diamonds) 295–300 s, (asterisks) 395–400 s, (diamonds uppermost) 495–500 s.

These curves exhibit three salient features. First, the decelerating downshifting of the peak is obvious except between the two latest curves, because the resolution in k space is too coarse to show it. Secondly, each of the data sets (save the initial condition) collapses onto the asymptotic power law decay. A best fit finds the spectral exponent to be $2\rho = 4.05$. Finally, the region of the spectrum below the spectral peak does not decay. This is an indication that the nonlinear interactions are pumping energy into this region, because the wind “driving” term is actually a wave damping term in this region.

[47] The strengths of the nonlinear interactions have been examined in detail. Figure 4 shows the third- and fourth-order terms in the equations of motion for ζ and ψ at two different wave numbers, one at approximately the spectral peak at the latest times, the other at nearly the largest k in the simulation. In both cases the third-order terms are considerably larger than the fourth-order terms. Also, however, the peak and high k cases are comparable in magnitude at third order, while at fourth order the peak case is roughly

an order of magnitude larger than the high case. There is a strong variability in all cases as a function of time. These results verify that the theory is operating in the “weakly nonlinear regime”, for if the fourth-order interaction were stronger than the third-order interaction, the systematic expansion procedure in powers of wave slope would be invalid.

3.3. Energy Considerations

[48] Figure 5 demonstrates the evolution of the energy density from $t = 500$ – 1000 s. It is remarkable that this quantity decreases for the first 750 s of the model run, and only starts growing past this time. The reason for this is that although the spectrum grows robustly in the downwind direction, it is heavily depleted in other directions as will be seen below. The original configuration was considerably more symmetrical. The lesson for future modeling is that the rate of depletion of waves in unfavorable conditions with respect to the wind may have to be diminished somewhat. Experimental guidance on the degree of wave damping due

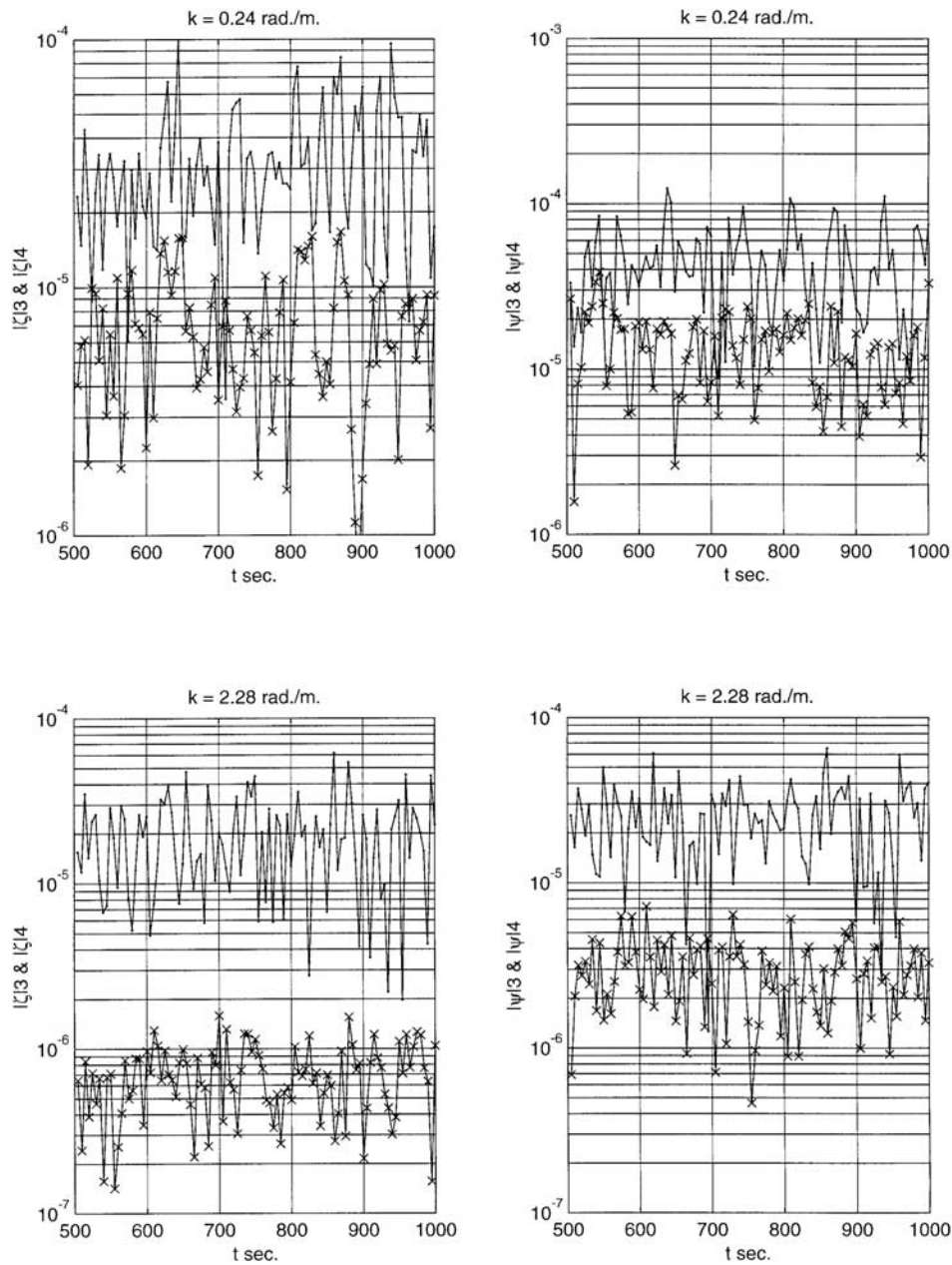


Figure 4. Temporal evolution of the nonlinear terms in the equations of motion. The abscissas are all in units of seconds. The ordinates are numerical values having the dimensions of the variables being plotted. The notation is as follows. The symbol $|\zeta|_3$ denotes the absolute value of the third order nonlinear interaction term (3) in the equation of motion for the displacement (ζ). Similarly, the symbol $|\psi|_4$ refers to the absolute value of the fourth order nonlinear interaction term in the equation of motion for the velocity potential, etc.

to adverse wind effects would be extremely helpful for addressing this issue realistically.

3.4. Angular Dependence of Spectrum

[49] Extraction of the angular dependence of the spectrum requires introduction of a further technique. The problem that arises is that the wave numbers form a square lattice. Thus to obtain the spectral value along a ray emanating from the origin requires interpolation of the values at the lattice points which surround the ray. At any fixed nontrivial angle the ray will traverse a series of

squares delineated by lattice points. If we select, say, 30 equally spaced $|k|$ values to sample each spectrum, each ray will have 30 tick marks. At each tick mark, linear interpolation is used to estimate the spectral value based on the three closest lattice points.

[50] Figure 6 displays the interpolated spectra as a function of polar angle for the peak wave number, an intermediate wave number, and approximately the maximum wave number. Notice that while the magnitudes are ordered in an expected manner for up to ~ 1.25 rad, a crossover occurs above that angle, with the peak k angular

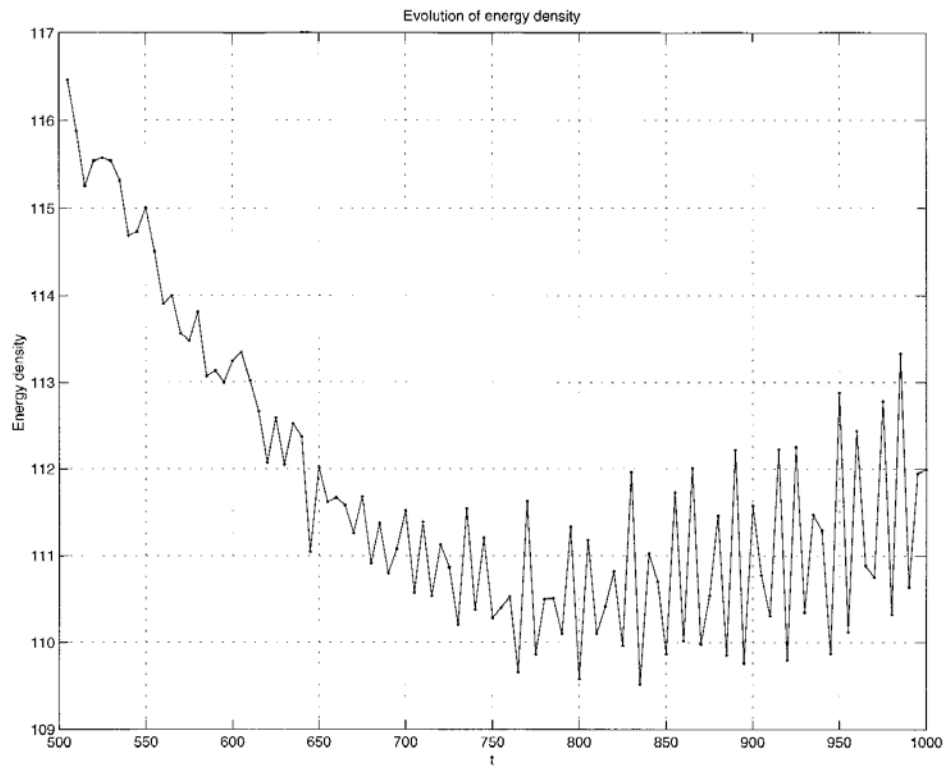


Figure 5. Total energy as a function of time.

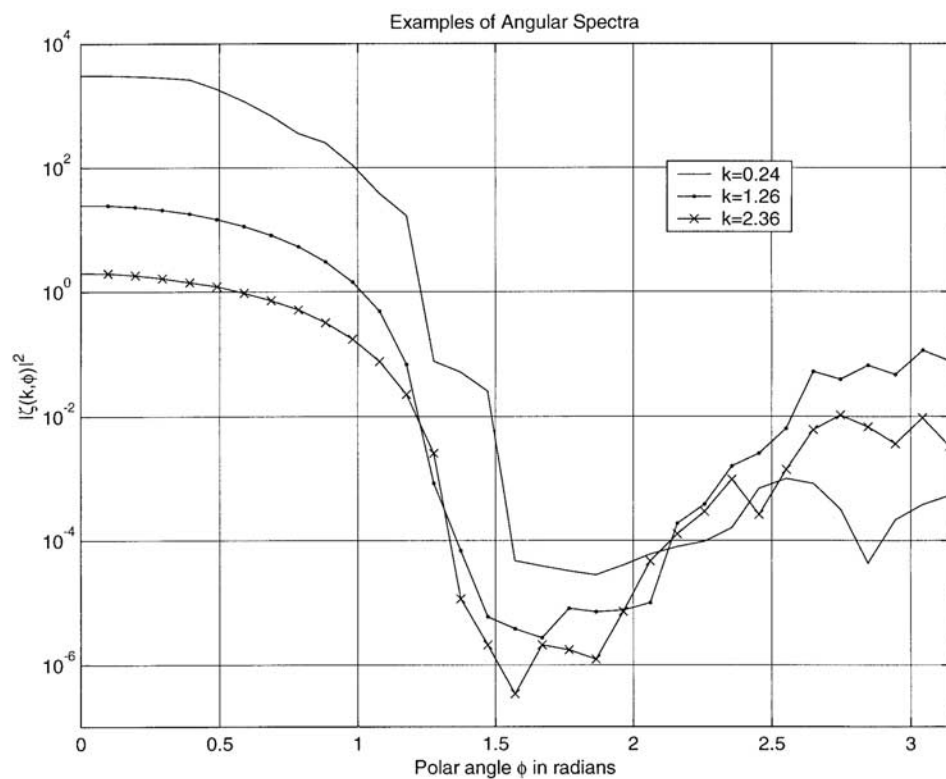


Figure 6. Directional spectra for three representative wave numbers as functions of angle. These are symmetric about $\varphi = 0$.

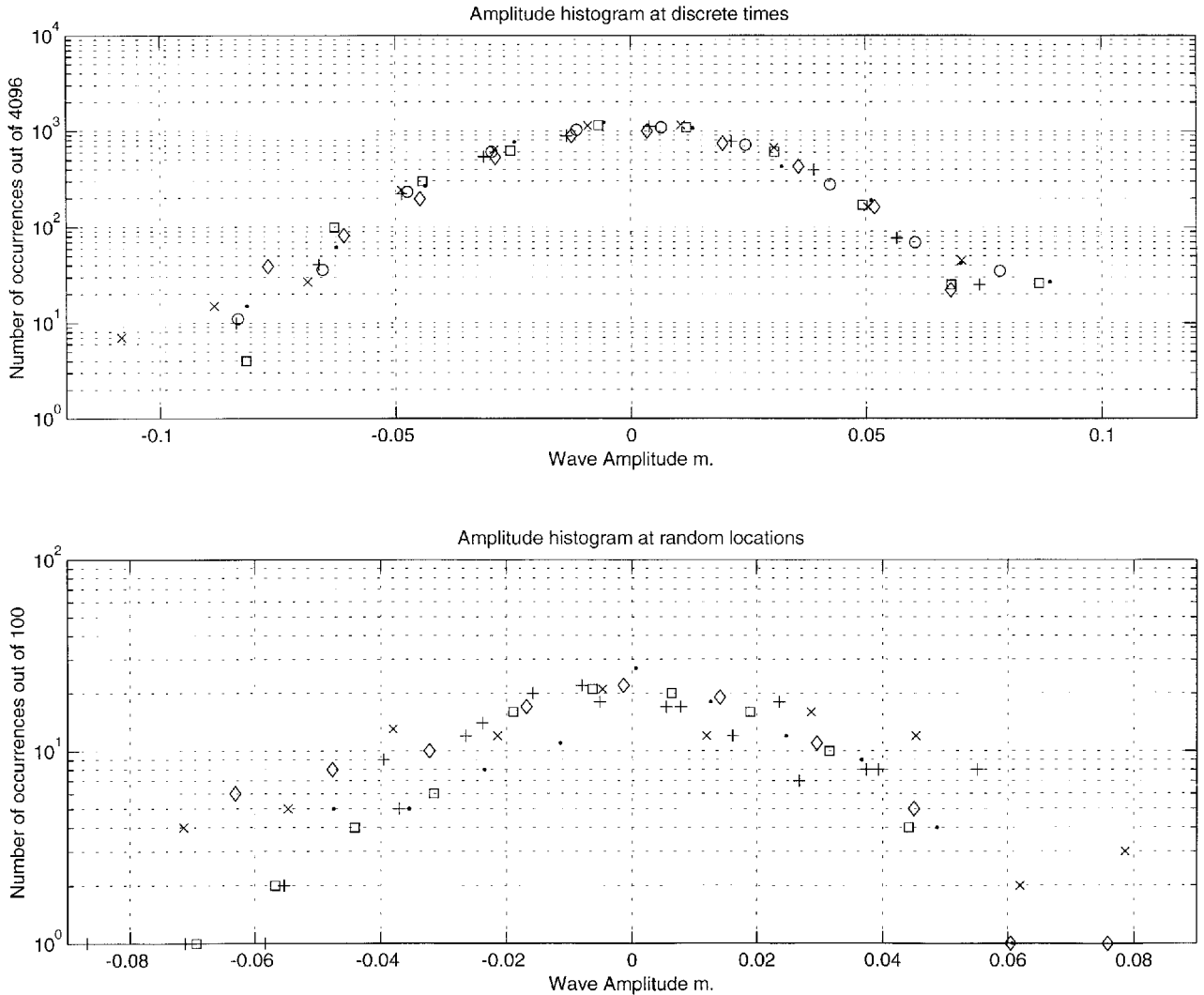


Figure 7. Wave amplitude frequencies of occurrence. (a) “Snapshot” of the wave field at discrete times ranging from 500 to 1000 s. in jumps of 100 s. The sampling is done across the spatial domain. (b) Samples drawn from “buoy” time series measurements at several randomly located spatial locations. In each case the distinct measurements are denoted by different symbols.

spectrum becoming the smallest component. Note also that the spectral components perpendicular to the wind direction are more heavily damped than the upwind components. The time series (not shown) reveal that the fully upwind component is actually growing in strength! This is due to the nonlinear interactions, as has been noted earlier.

[51] A straightforward average over 64 angles gives a very good fit with spectral exponent: 3.91. The downwind component is so significantly larger than any of the others that it dominates the average.

3.5. Wave Statistics

[52] Figure 7 shows two different ways of constructing the wave amplitude probability distribution function (pdf) on the basis of our numerical data. Figure 7 (top) corresponds to taking a snapshot of the wave field over the entire spatial range. Figure 7 (bottom) corresponds to monitoring the time evolution at a fixed location, as on a buoy.

[53] There exists considerably more scatter in Figure 7 (bottom) than in Figure 7 (top) because the time series that were examined contained only 100 points, while the “photos” in Figure 7 (top) contained 4096 pixels. Nonetheless, both have roughly the “bell shape” characteristic of a true Gaussian distribution, except at the extreme ends (deepest troughs and highest crests).

[54] Figure 8 extends this analysis by averaging over a 5-s interval. The circles denote the data, while the dots denote a fit of a Gaussian function with zero mean and variance equal to that in the data. It is evident that these averaged data deviate significantly from Gaussian behavior albeit they have the same general shape. Let us explore this in detail.

[55] Quantitatively, given a normalized Gaussian pdf, the total probability of having waves larger than 2σ , where σ denotes the standard deviation, is given by $\text{erfc}(\sqrt{2}) = 0.046$. At times of 500, 750, and 1000 s, the fraction of such points was found to be 0.075, 0.101, and 0.056,

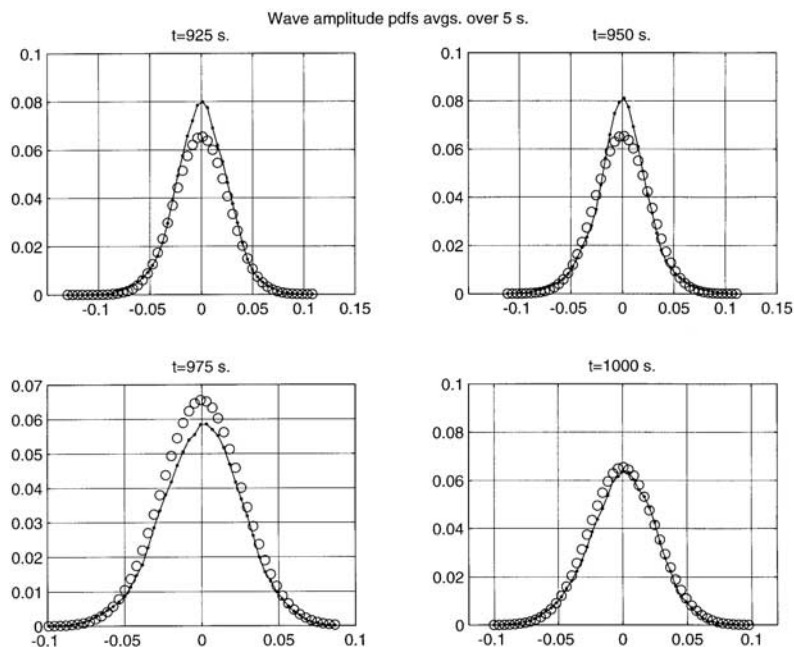


Figure 8. Wave amplitude probability distribution functions averaged over 5 s at 4 different “late” times. The circles denote the numerical results, while the points denote Gaussian functions with zero mean and variance equal to that of the numerical data.

respectively. These results suggest that the phase-retaining equations lead to a significantly larger fraction of extreme events than a Gaussian distribution should support, although further investigation is required to quantify this observation more accurately.

[56] A second measure of the wave statistics may be introduced by reconstructing the spatial wave field using the calculated $|\zeta(k, t)|$ multiplied by a random phase for each value of k . We call this a “synthetic” wave field. Introduce the moments

$$m_r = \sum_i (h_i - \langle h \rangle)^r / N,$$

where h_i are the heights at locations i and N is the total number of locations. Then the skewness is defined to be $m_3 / (m_2)^{3/2}$, while the kurtosis is $m_4 / (m_2)^2$. Theoretically, a Gaussian distribution has skewness equal to zero and kurtosis equal to 3. For 100 realizations of the synthetic wave field the mean skewness is found to be -0.02 with a standard deviation of 0.14, and the mean kurtosis is 2.95 with a standard deviation of 0.25. These results are consistent with a Gaussian pdf.

[57] The wave field constructed from the calculated $\zeta(k, t)$ retaining the phase produced by the calculation yields different values. When averaged over 100 times, the skewness is -0.11 with standard deviation 0.22 while the kurtosis is 3.35 with standard deviation 0.54. Nevertheless, the large standard deviations in the synthetic and “true” quantities indicate that statistically, they overlap. In other words, by this test it is not inconsistent to say that the phases have become randomized after 500 s of evolution.

[58] Figure 9 shows the temporal development of the skewness and kurtosis of the true wave field. The main

point to observe is that while these quantities are generally close to the Gaussian values, there are episodic large fluctuations. (The $\langle h \rangle$ over these realizations is not plotted as it has a numerical value at the level of machine noise, as it should.)

[59] Finally, wave statistics are often characterized in terms of the following linear combination of ζ and ψ :

$$a(k, t) = \frac{1}{\sqrt{2}} \left[\left(\frac{g}{k} \right)^{1/4} \zeta(k, t) + i \left(\frac{k}{g} \right)^{1/4} \psi(k, t) \right].$$

This linear combination is useful, because, for example, the wave action takes the simple form $A(t) = \int dk a^*(k, t) a(k, t)$.

[60] Now, under the assumption of Gaussian statistics, $\langle a^*(k', t) a(k, t) \rangle = F(k) \delta(k' - k)$, where the averaging symbols $\langle \cdot \rangle$ formally refer to integrating over the Gaussian pdf. In practice, of course, the average must be performed at a given time by sampling many different sites, or by performing a time average at a given site. Figure 10 represents a time average of the action density over a 5-s interval from 950 to 1000 s of wave evolution. It is very sharply peaked about zero lag, in accordance with Gaussian statistics.

[61] Next, as an example of a triple moment, examine $\langle a^*(k', t) a(k, t) a(k, t) \rangle$. Figure 11 unambiguously shows that this moment has a strong zero-lag peak and a secondary peak at positive lag as well. While the reason for the location of the second peak requires further thought, the crucial point is that this moment must vanish identically for all k and k' under Gaussian statistics. Its failure to do so negates the possibility of directly comparing the results from this model to WAM-type results based on the same initial conditions. (The plot shows the absolute value of the average and not the average of the absolute value. The

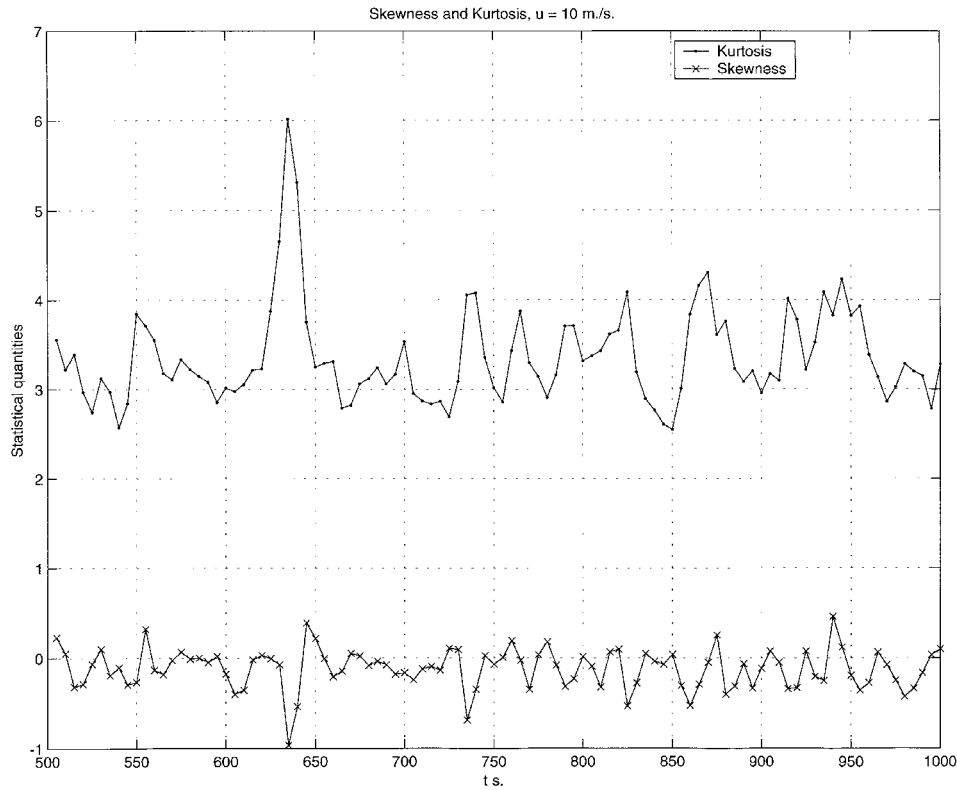


Figure 9. Skewness and Kurtosis coefficients as functions of time.

asymmetry of the secondary peak is due to the precise triple moment taken. The complex conjugate of the term displayed yields a peak at negative lag.)

[62] It is important to note that the moments depicted in Figures 10 and 11 are normalized to have a maximum value of unity. However, the “raw” unnormalized peak heights are $2.42e3$ for the second moment, and $3.47e4$ for the third.

We have not, therefore, exaggerated the importance of the third moment by normalization.

3.6. Numerically Observed Growth Time Constants

[63] The growth rates observed experimentally are not identical to their theoretically predicted values. This is because the wave field is never simply growing, nor simply

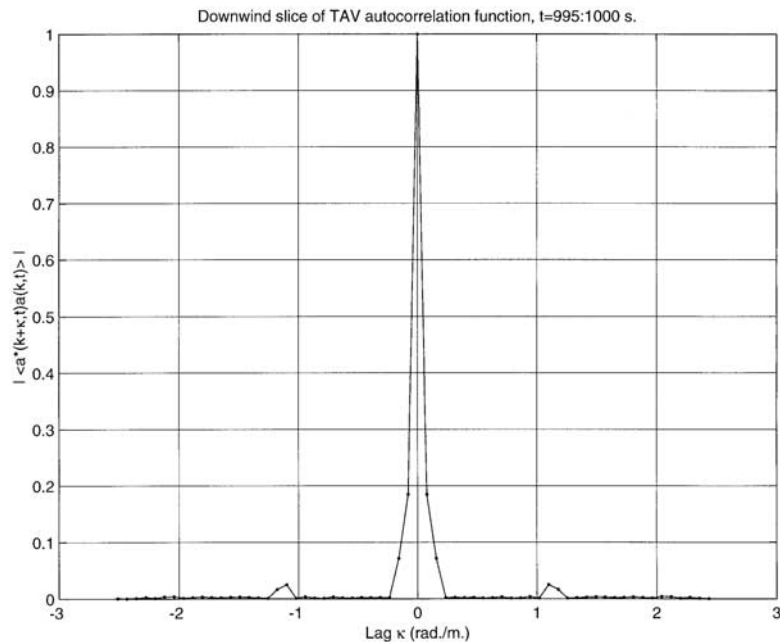


Figure 10. Autocorrelation function of the variable $a(k, t)$ (see text for definition), averaged over the 5 s interval between 995 and 1000 s, normalized so that the maximum value is 1.

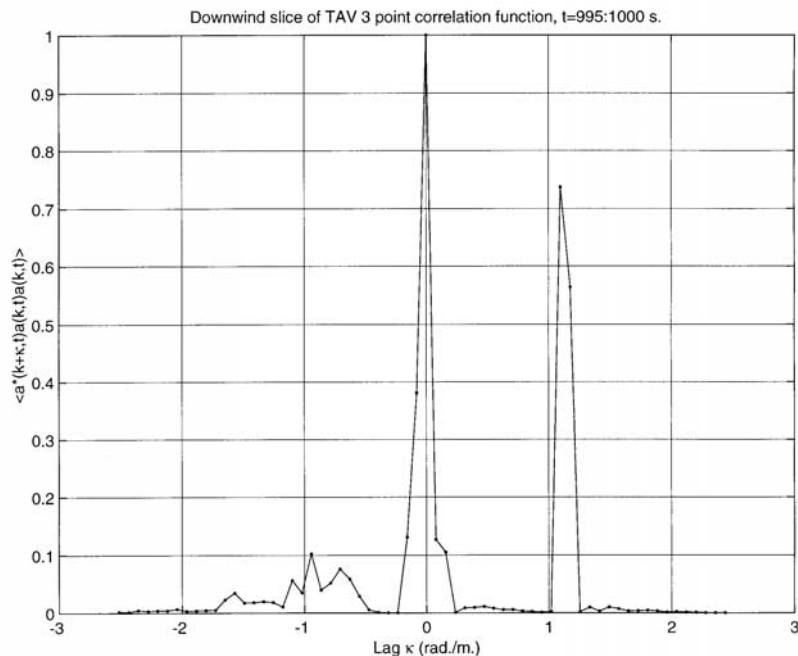


Figure 11. Three point correlation function averaged over the 5-s interval between 995 and 1000 s, normalized so that the maximum value is 1.

dissipating. These two processes are acting simultaneously. In addition nonlinear exchange is constantly taking place; we have discussed evidence of its importance in keeping the “forward face” of the spectrum from vanishing altogether. Consequently what one observes experimentally is an “effective” growth rate, which turns out to be exponential in time over only a limited time span depending on wave number.

[64] To examine growth rates from the simulations quantitatively, we introduce time-averaged spectra over 5-s intervals, as was introduced earlier. The reason for this is that it is quite difficult to extract a pure exponential growth dependence when the spectra also contain a strong oscillatory component. Time averaging smoothes out this latter component, as can be seen directly from Figure 12, which exhibits two cases for which an exponential fit has been applied to the raw data sets in the windward direction. As noted above, exponential growth occurs over relatively early times, after which the spectra saturate. Furthermore, with increasing wave number the “exponential” regime shrinks considerably; the time constants are smaller and saturation sets in earlier. This is exactly as was observed by *Willemsen* [1997] from SWADE data.

[65] Table 1 displays results obtained for a range of wave numbers using figures such as Figure 12. Before examining the table, however, note that in the absence of nonlinear interactions and dissipation, the equations of motion yield

$$\zeta \text{ and } \psi \propto \exp(t/2\tau_{\text{calc}}) \exp(\pm i\omega_k t),$$

so $|\zeta(k, t)|^2$ grows as $\exp(t/\tau_{\text{calc}})$. Here τ_{calc} is obtained as in Figure 1. For purposes of comparison, the model has been run including driving and dissipation but no nonlinear interactions. It is interesting to observe that the simulation values are close to the “linear” model values, and also close but not identical to the “theoretical” values based on the DP growth model.

[66] These results indicate that in the absence of nonlinear terms, the growth rates obtained from the numerical experiment are in excellent agreement with the rates predicted from the functional form of the driving term. They do not agree precisely because dissipation limits the range over which these growth rates can be calculated as well as influencing the net growth rate itself.

[67] Once the nonlinear interactions are introduced, the growth time constant is in all cases significantly different from the predicted rates. The discrepancy is not, however, uniform. At the lowest wave number in the table (for which c_k is still less than 10 m s^{-1}) the time constant is smaller than the predicted value. This indicates that these waves are growing not only in response to the wind, but also because of the spectral cascade caused by the nonlinear interactions. From the approximate position of the peak at near “full development” upward in k , the time constants are longer than the predicted values.

[68] This is also due to the nonlinear cascade. The cascade works toward the direction of low wave numbers, thus depleting energy from higher wave numbers. The amount of energy transported from any given region depends on the energy available in that region. So the downshift from the vicinity of the spectral peak, wherever it is at any given time, is strong. However, the drift into the vicinity of the peak is small. Thus the net effect of the nonlinear interactions is to deplete the vicinity of the peak. This region still grows, of course, but more slowly than it does in the absence of nonlinear interactions.

4. Summary and Conclusions

4.1. Results of Investigation

[69] In this paper we have studied a model for ocean wave evolution under driving and dissipation retaining

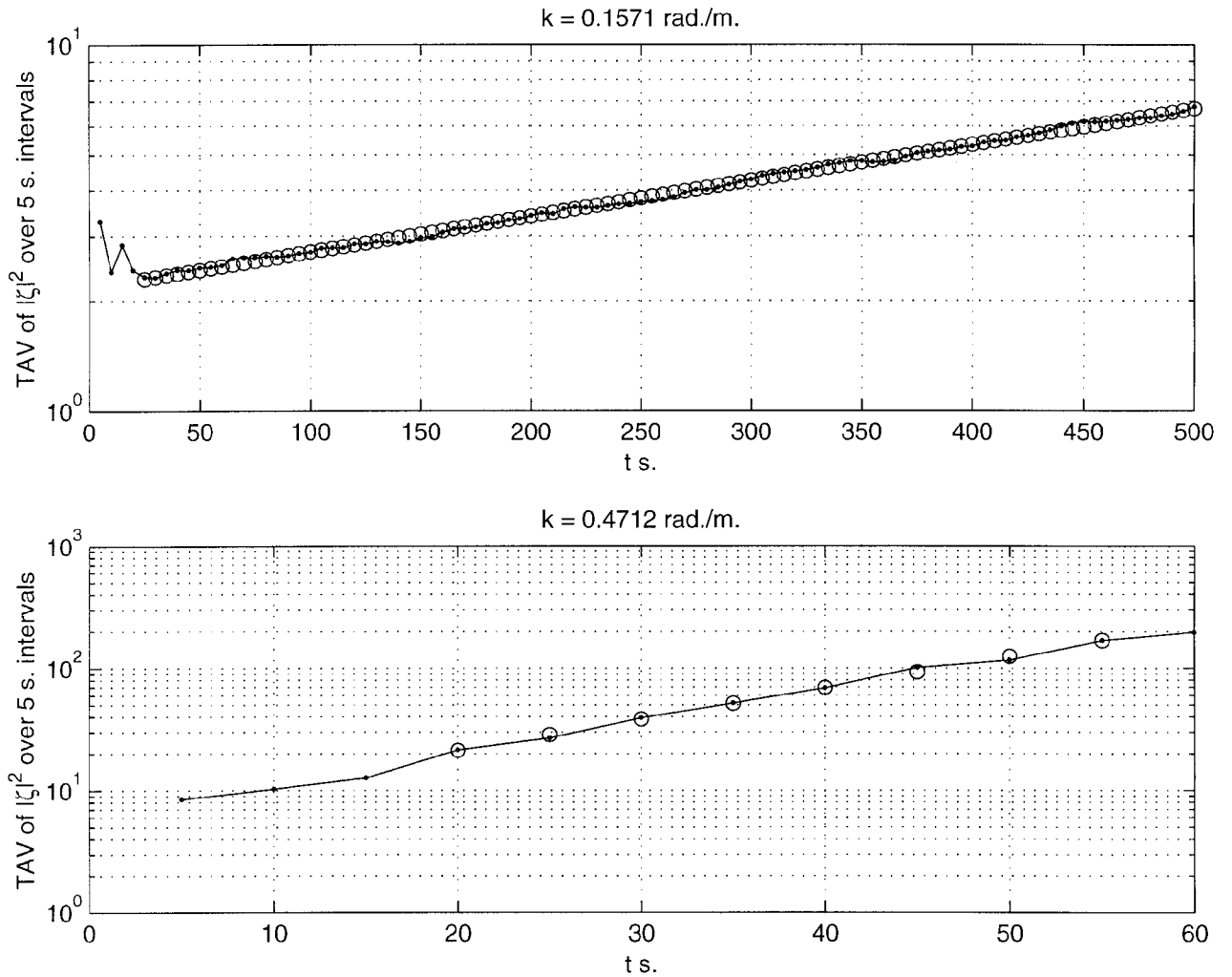


Figure 12. Exponential fits to the growth curves at the high and low wave numbers cited in Table 1. The dots represent the simulation-generated data, while the circles represent the fit.

third- and fourth-order nonlinear interactions. We have found the following results.

[70] The spectral peak shifts to lower wave numbers in response to wind driving. This shift rate itself is a function of time/fetch/wave age. The results provide physical insight into the causes of this downshift which have not been emphasized by previous workers; the nonlinear interactions certainly participate in determining the rate of the shift, but the k dependence of the driving term plays a crucial role as well. The rate of the drift was quantified in $d = 1$ [Willemssen, 2001b], and it can be quantified in $d = 2$ as well, using more wave numbers.

[71] The spectrum develops an asymptotic power law tail. It has been found that the asymptotic spectral exponent in the down-wind direction is sensitively dependent on the form of the dissipation function. This result was obtained using computationally determined scalings, and it is quite different from what would have been anticipated based on earlier formulations. Straightforward comparison with transport formulations is complicated by the fact that odd moments are nonvanishing (section 3.5), thus negating the possibility of concluding that our results correspond to a Gaussian pdf. One would be comparing “apples to oranges”.

[72] Qualitatively realistic angular distributions have been produced in the course of the calculations but it remains to be seen if they are quantitatively realistic. Note that in addition to the peak region, the asymptotic part of the spectrum is also angle dependent. Recall that the dissipation-spectrum relationship was established using the down-wind spectrum.

[73] The calculations allow for an unambiguous quantification of the degree of spectral mixing due to nonlinear interactions within the original canonical variable formulation prior to the transformation that eliminates nonresonant three wave interactions. We have found that these interactions act in concert with the dissipation function to build a long power law spectral tail. Additionally they fill

Table 1. Theoretical and Observed Growth Constants

K , rad/m	τ_{calc} , S	τ_{linear} , S	τ_{nonlin} , S
0.1571	455.9	455.6	436.5
0.2356	86.9	87.2	90.9
0.3141	36.5	37.1	39.7
0.3926	20.3	20.9	24.5
0.4712	13.1	13.8	15.9

in portions of the spectrum below the spectral peak which are depleted by the growth term under unfavorable conditions.

[74] The consistency of the small slope expansion has been tested by comparing the third-order interactions and the fourth-order interactions. The latter are systematically smaller than the former. As shown by *Willemsen* [2000b], however, the near resonances sustained by the fourth-order interactions do give rise to harmonics when a narrow band spectrum is employed as an initial condition. These are smoothed out by the dissipation term and by “spectral promiscuity”. This latter term refers to a process under which partners in a resonant quartet find new partners to resonate with, which then find yet other partners, etc., thus spreading the energy across the spectrum. Once a quasi-steady state has been reached, exchanges among resonant quartets persist but they no longer produce sharp peaks.

4.2. Future Directions

[75] The work done to date can readily be expanded in a number of important directions. Construction of a physical interpretation of the dissipation mechanism is sorely needed. What we have in mind here are steps along the lines taken by *Phillips* [1985], which established a possible connection between the form of the dissipation term in the transport formalism and the whitecap coverage. *Belcher and Vassilicos* [1997] work this differently, combining a statistical model for how waves break in space with scaling properties of the dissipation to obtain k^{-4} asymptotics. (This work is possibly in need of key supportive experimental observations, but it illustrates how *Phillips* [1985] is not iron-clad in his prediction of the dissipation term.) Although our dissipation model yields the same spectral falloff, it is not identical with either Phillips or Belcher-Vassilicos, so the physical interpretation may be different. The manner in which this physical interpretation relates to the correlation we have found between dissipation and the nonlinear interactions remains to be seen.

[76] The initial condition may be any sea state one desires; that is, there may be preexisting waves of any specified form. For example, one may envision winds starting up over a sea which contains one or more swell contributions from previous storms. The calculations can be run under such conditions with no modifications to the code. It is entirely possible that such initial conditions will yield results in much better agreement with Gaussian statistics, for it is just such conditions which are invoked to justify the random-phase approximation in the first place.

[77] We can incorporate changes in mean wind speed and direction. While this is generally true, it is also feasible within the Matlab environment because the wind may be a function of time both in magnitude and direction without significantly altering any aspect of the calculational scheme. These changes are not restricted to overall changes in the wind field. While very short duration wind fluctuations are not expected to alter the wave growth except for waves with periods of comparable duration, longer scale gustiness may be introduced into the model.

[78] As was discussed extensively, the DP driving term is convenient to use for demonstration purposes. Further research can incorporate more sophisticated expressions such as those of *Cohen and Belcher* [1999].

[79] The model to this point is not, however, entirely complete. First, an important feature of spectral evolution that has not been reproduced in the model is the phenomenon of “overshoot.” *Tolman and Chalikov* [1996] found it useful to introduce a modification of the dissipation term which operates primarily in the vicinity of the spectral peak in order to achieve this overshoot, and similar modifications can be introduced within the deterministic formulation as well. Additionally, *Banner* [1990] has observed a dependence of the absolute amplitude of the wave number spectrum which scales on C_{peak} . The calculations reported here do not exhibit this scaling in the tail regions. We do not view this as a drawback but rather as a challenge; we will need more wave numbers and longer times to address this issue.

[80] Finally, we have not discussed capillary waves, currents, or depth dependencies in this work. *Pushkarev and Zakharov* [1996, 2000] have discussed the former using deterministic equations, and derived their spectral behavior. However, the characterization of capillary waves in the presence of gravity waves may benefit from utilization of novel techniques, as given by *Henyei et al.* [1988] and *Creamer et al.* [1989]. Depth dependence of the Krasitskii equations was given by Krasitskii himself [*Krasitskii*, 1994] in the case of constant bathymetry. Variable bathymetry has been investigated within the deterministic framework by a number of authors, [e.g., *Smith*, 1998]. A first step toward dealing with wave-current interactions is to make a Galilean transformation into a frame co-moving with the current. However, since currents are variable, further in-depth research is required. All of these considerations are beyond the scope of the present work.

[81] **Acknowledgments.** It is a pleasure to thank Michael Brown, Mark Donelan, and Michael Stiassnie for useful discussions and suggestions. This work was funded in its entirety by the Rosenstiel School of Marine and Atmospheric Science.

References

- Al-Zanaidi, M. A., and W. H. Hui, Linear dynamics of wind waves in coupled turbulent air-water flow, 1, Theory, *J. Fluid Mech.*, 148, 225–246, 1984.
- Balkovsky, E., G. Falkovich, and A. Fouxon, Intermittent distribution of inertial particles in turbulent flows, *Phys. Rev. Lett.*, 86, 2790–2793, 2001.
- Banner, M. L., Equilibrium spectra of wind waves, *J. Phys. Oceanogr.*, 20, 966–984, 1990.
- Banner, M. L., and I. R. Young, Modeling spectral dissipation in the evolution of wind-waves, 1, Assessment of existing model performance, *J. Phys. Oceanogr.*, 24, 1550–1571, 1994.
- Banner, M. L., and X. Tian, On the determination of the onset of breaking for modulating surface gravity water waves, *J. Fluid Mech.*, 367, 107–137, 1998.
- Baumann, G., N. Sudland, and T. F. Nonnenmacher, Anomalous relaxation and diffusion processes in complex systems, *Transp. Theory. Stat. Phys.*, 29, 157–171, 2000.
- Belcher, S. E., and J. C. R. Hunt, Turbulent shear flow over slowly moving waves, *J. Fluid Mech.*, 251, 109–148, 1993.
- Belcher, S. E., and J. C. Vassilicos, Breaking waves and the equilibrium range of wind-wave spectra, *J. Fluid Mech.*, 342, 377–401, 1997.
- Cohen, J. E., and S. E. Belcher, Turbulent shear flow over fast-moving waves, *J. Fluid Mech.*, 386, 345–371, 1999.
- Creamer, D. B., et al, Improved linear representation of ocean surface waves, *J. Fluid Mech.*, 205, 135–161, 1989.
- Donelan, M. A., and W. J. Pierson, Radar scattering and equilibrium ranges in wind-generated waves with application to scatterometry, *J. Geophys. Res.*, 92(C5), 4971–5029, 1987.
- Donelan, M. A., Wind-induced growth and attenuation of laboratory waves, in *Wind-over-Wave Couplings*, edited by S. G. Sajjadi, N. H. Thomas, and J. C. R. Hunt, pp. 183–194, Clarendon, Oxford, England, 1999.

- Hara, T., and C. C. Mei, Frequency downshift in narrowbanded surface-waves under the influence of wind, *J. Fluid Mech.*, 230, 429–477, 1991.
- Henye, F. S., et al, The energy and action of small waves riding on large waves, *J. Fluid Mech.*, 198, 443–462, 1988.
- Kitalgorodskii, S. A., Application of the theory of similarity to the analysis of wind-generated waves as a stochastic process, *Bull. Acad. Sci. USSR Geophys. Ser.*, 1, 73 pp., 1962.
- Komen, G. J., et al., *Dynamics and Modeling of Ocean Waves*, 532 pp., Cambridge Univ. Press, New York, 1994.
- Krasitskii, V. P., On reduced equations in the Hamiltonian theory of weakly nonlinear surface waves, *J. Fluid Mech.*, 272, 1–20, 1994.
- Landau, L., and E. M. Lifshitz, *Mechanics*, Addison-Wesley, Reading, Mass., 1960.
- Lin, R. Q., and N. E. Huang, The Goddard coastal wave model, 1, Numerical method, *J. Phys. Oceanogr.*, 26, 833–847, 1996a.
- Lin, R. Q., and N. E. Huang, The Goddard coastal wave model, 2, Kinematics, *J. Phys. Oceanogr.*, 26, 848–862, 1996b.
- Magnusson, A. K., M. A. Donelan, and W. M. Drennan, On estimating extremes in an evolving wave field, *Coastal Eng.*, 36, 147–163, 1999.
- Phillips, O. M., Spectral and statistical properties of the equilibrium range in wind-generated gravity waves, *J. Fluid Mech.*, 156, 505–531, 1985.
- Pushkarev, A. N., and V. E. Zakharov, Turbulence of capillary waves, *Phys. Rev. Lett.*, 76, 3320–3323, 1996.
- Pushkarev, A. N., and V. E. Zakharov, Turbulence of capillary waves: Theory and numerical simulation, *Physica D*, 135, 98–116, 2000.
- Smith, R. A., An operator expansion formalism for nonlinear surface waves over variable depth, *J. Fluid Mech.*, 363, 333–347, 1998.
- Su, M. Y., et al., Developing a joint Army/Navy coastal wave prediction program: A planning report, *Tech. Rep. NRL/MR/7330-95-7686*, 103 pp., Nav. Res. Lab., Stennis Space Center, Miss., 1996.
- Tolman, H. L., and D. Chalikov, Source terms in a third-generation wind wave model, *J. Phys. Oceanogr.*, 26, 2497–2518, 1996.
- Willemsen, J. F., Analysis of SWADE discus N wind speed and wave height time series, II, Quantitative growth rates during a storm, *J. Atmos. Oceanic Technol.*, 14, 630–643, 1997.
- Willemsen, J. F., Enhanced computational methods for nonlinear Hamiltonian wave dynamics, *J. Atmos. Oceanic Technol.*, 15, 1516–1522, 1998.
- Willemsen, J. F., Enhanced computational methods for nonlinear Hamiltonian wave dynamics, II, New results, *J. Atmos. Oceanic Technol.*, 18, 775–790, 2001a.
- Willemsen, J. F., Deterministic modeling of driving and dissipation for ocean surface gravity waves, *J. Geophys. Res.*, 106(C11), 27,187–27,204, 2001b.
- Zakharov, V. E., On instability of waves in nonlinear dispersive media, *Sov. Phys. JETP*, 51, 1107–1114, 1966.
- Zakharov, V. E., Stability of periodic waves of finite amplitude on the surface of a deep fluid, *J. Appl. Mech. Tech. Phys.*, 9, 190–194, 1968.
- Zakharov, V. E., Hamiltonian formalism for waves in nonlinear dispersive media, *Izv. Vyssh. Uchebn. Zaved. Radiofiz.*, 17, 431–453, 1974.

J. F. Willemsen, Rosenstiel School of Marine and Atmospheric Science, University of Miami, 4600 Rickenbacker Causeway, Miami, FL 33149, USA. (jwillemsen@rsmas.miami.edu)